Pomeron and multiparticle production

I. Kawrakow
Fachbereich Physik, Universität Leipzig, Federal Republic of Germany
(Received 10 September 1993)

A new model for high energy hadron-hadron interactions based on the Pomeron containing both "soft" and perturbative contributions is presented. Its intercept is expressed through the intercept of the Reggeized gluon. The multigluon intermediate state of hadronic interactions is obtained from the equation of the perturbative QCD Pomeron. Implementing the model in a Monte Carlo event generator, a systematic study of a broad range of data in a wide energy range is performed. The energy dependence of rapidity and transverse momentum spectra, the violation of the Koba-Nielsen-Olesen scaling of multiplicity distribution, and the increase of the correlations among final state particles are shown to be simultaneously well described. Predictions of the model up to the energies of the future supercolliders are given.

PACS number(s): 13.85.Hd, 12.39.−x, 12.40.Nn

I. INTRODUCTION

It has been suggested by many authors that the production of jets with transverse momenta of a few GeV (minijets), although not resolvable in distinct jets, may be at least partially responsible for a variety of phenomena in high energy hadronic interactions, such as the rise of the total cross section and the height of the pseudorapidity plateau with increasing energy, the violation of the Koba-Nielsen-Olesen (KNO) scaling of multiplicity distribution, the growth of the average transverse momentum, and the two-particle correlation strength [1–9]. Several Monte Carlo models have been developed to take the minijet component of hadronic interactions into account [7,10–12]. However, in all these models, the lowest-order matrix elements of perturbative QCD (PQCD) together with the parton model are used to calculate the cross section for parton-parton scattering with a minimum momentum exchange $p_\perp^{\text{cutoff}}$ (introduced in order to avoid infrared divergencies), and a phenomenological "K factor" is applied to account for higher-order corrections. The models differ in the assumptions applied in the calculation of the relative weight of the PQCD processes as compared to the "soft" ones. In some of the models (HIJING [10], PYTHIA [11]) initial and final state evolution of the partons participating in a hard interaction is performed.

In this paper I present a new model based on the Regge asymptotics of PQCD in the leading logarithmic approximation (LLA) [13–15] and the perturbative Reggeon calculus [16], combined with a very simple phenomenological ansatz to convert the "s"-channel multigluon intermediate state of the Pomeron into final state hadrons. In many aspects the model is guided by basic ideas of the dual parton model (DPM) [17–20] (for a recent review see Ref. [21]). Let me emphasize the main new features of this new model: All orders of PQCD in the LLA are simultaneously taken into account; the Pomeron contains the contributions from both PQCD and "soft physics." Its intercept can be expressed through the intercept of the Reggeized gluon.

These two features will be discussed in more detail in the next section, where the basic equations describing the perturbative Pomeron (PP) are presented. In Sec. II A the equation of the PP is used to construct a simulation procedure for the multigluon intermediate state of the PP. The coupling of the QCD ladder to the hadrons is discussed in Sec. II B: With a simple ansatz a formula is found, describing the energy dependence of the total cross section for Pomeron exchange and the relative weights of the "soft" and perturbative contributions. In Sec. III is shown how unitarity corrections to the single Pomeron amplitude can be taken into account and the model parameters are fixed from a fit to the total and elastic cross sections in pp and $p\bar{p}$ collisions. In Sec. IV the transition of the multigluon intermediate state of the Pomeron into hadrons is discussed. In Sec. V the model results are compared with existing experimental data. Finally, Sec. VI concludes with a summary.

II. THE POMERON

Recently it has been shown by Fippel and Kirschner how the PP equation can be used to obtain a simulation procedure for the intermediate multigluon state of high energy hadronic interactions [22]. Then the authors of Ref. [22] construct a simple model for multiparticle production reproducing well the rise of the average charged multiplicity and the height of the pseudorapidity plateau in $p\bar{p}$ interactions in the range from 60 GeV to 1.8 TeV. Although this section is partially based on the results of Ref. [22], I present the basic equations because of their importance for the further discussion. Furthermore, contrary to the results of Ref. [22], I find that the s-channel hadronic intermediate states contributing to the PP show rising rapidity distributions with increasing energy (see Sec. V and for more details Ref. [23]).

The Regge asymptotics of QCD has been investigated in the LLA in Refs. [13–15]. In this approximation the PP results from a sum of generalized gluon ladder graphs. The two gluons exchanged in the t channel are Reggeized

gluons with the trajectory $1+\alpha(\kappa)$:

$$\alpha(\kappa)=\frac{g^2N}{2(2\pi)^3}\kappa^2\int\frac{d^2\kappa'}{|\kappa-\kappa'|^2\kappa'^2}\ . \tag{1}$$

In the above expression g is the QCD coupling and N the number of colors. The leading logarithms arise if the momenta of the s-channel gluons (k_i-k_{i+1}) obey the conditions of multi-Regge kinematics. In terms of Sudakov components

$$k_i=\alpha_i p_2+\beta_i p_1+\kappa_i,\quad 2p_1p_2=s, p_1^2=p_2^2=0, \tag{2}$$

these conditions read

$$\begin{aligned}&|\alpha_{i+1}|\gg|\alpha_i|,\\ &|\beta_{i+1}|\ll|\beta_i|,\\ &\alpha_i\beta_i s\ll\kappa_i^2,\\ &\alpha_{i+1}\beta_i s\simeq-\kappa_i^2.\end{aligned} \tag{3}$$

In the following we set $\alpha_i<0$ and $\beta_i>0$. The Pomeron equation is usually formulated in terms of t-channel partial waves, related in the high energy asymptotics to the Pomeron amplitude $\mathcal{A}(s,q,\kappa)$ by Mellin transformation:

$$\mathcal{A}(s,q,\kappa)=\int_{-i\infty}^{i\infty}\frac{d\omega}{2\pi i}f(\omega,q,\kappa)\left(\frac{s}{s_0}\right)^\omega \tag{4}$$

with the partial-wave equation

$$\begin{aligned}f(\omega,q,\kappa)=\ &f_0(\omega,q,\kappa)+\frac{g^2N}{(2\pi)^3\omega}\int\frac{d^2\kappa'}{\kappa'^2(q-\kappa')^2}\left(-q^2+\frac{(q-\kappa')^2\kappa^2+\kappa'^2(q-\kappa)^2}{\kappa-\kappa'^2}\right)f(\omega,q,\kappa')\\ &-\frac{g^2N}{(2\pi)^3 2\omega}\int\frac{d^2\kappa'}{(\kappa-\kappa')^2}\left(\frac{\kappa}{\kappa'^2}+\frac{(q-\kappa)^2}{(q-\kappa')^2}\right)f(\omega,q,\kappa)\end{aligned} \tag{5}$$

with s_0 being the hadronic scale, q the momentum transfer, and $f_0(\omega,q,\kappa)$ the driving term for the perturbative expansion,

$$f_0(\omega,q,\kappa)=\frac{g^2N}{\omega}. \tag{6}$$

The leading singularity of the partial wave in the complex angular momentum plane determines the asymptotic behavior of the scattering amplitude and was found in Refs. [24, 25] to be a branch point located at $1+\Delta$, with

$$\Delta=\frac{g^2}{\pi^2}N\ln 2=12\ln 2\frac{\alpha_s}{\pi}\sim 0.5,\quad \alpha_s\sim 0.2\ . \tag{7}$$

This is the famous "intercept of the QCD Pomeron" leading very quickly to violation of unitarity. However, if we consider real processes between hadrons the amplitude $\mathcal{A}(s,q,\kappa)$ has to be integrated over κ together with an unknown nonperturbative function $G_1(x_1,\kappa)G_2(x_2,\kappa)$, where $G_i(x,\kappa)$ describe the coupling of the QCD ladder to a parton from the hadron h_i with the momentum fraction x_i and the virtualness κ. This problem will be addressed in the second part of this section.

A. The multigluon states of the QCD Pomeron

First, I critically review the simulation procedure for the multigluon intermediate state of the PP introduced in Ref. [22]. Let me consider the imaginary part of the elastic scattering amplitude for zero momentum exchange,

$$A(s,\kappa)=\mathrm{Im}\mathcal{A}(s,q=0,\kappa), \tag{8}$$

for two off-shell partons having the four-momenta p_1', p_2' with

$$p_1'^2, p_2'^2=-\kappa^2, (p_1'+p_2')^2=s. \tag{9}$$

Up to normalization factors $A(s,\kappa)$ gives the total cross section. Then Eq. (5) simplifies to

$$f(\omega,\kappa)=f_0+\frac{g^2N}{(2\pi)^3\omega}\int\frac{d^2\kappa'}{\kappa'^2}\frac{2\kappa^2}{|\kappa-\kappa'|^2}f(\omega,\kappa')-\frac{2}{\omega}\alpha(\kappa)f(\omega,\kappa)\ . \tag{10}$$

Inverting the Mellin transformation, a power of ω becomes a derivative with respect to $\ln s_0/s$ and we get [22]

$$\frac{d}{d\ln s_0/s}A(s,\kappa)=\frac{2g^2N}{(2\pi)^3}\kappa^2\int\frac{d^2\kappa'}{\kappa'^2|\kappa-\kappa'|^2}A(s,\kappa')-2\alpha(\kappa)A(s,\kappa)\ . \tag{11}$$

Note that the infrared singularities on the right-hand side cancel each other. For the numerical simulation it is convenient to introduce a cutoff parameter μ in order to regularize the singularities in both terms demanding

$$\kappa'^2, |\kappa-\kappa'|^2\geq\mu^2. \tag{12}$$

Note that in addition to regularizing the two terms of Eq. (11), μ also determines the lowest possible subenergy $s_i\geq\mu^2$. Furthermore, in order to guarantee the applicability of the perturbative result, μ has to be of the same order as the hadronic scale, i.e., $\mu\sim s_0$. Therefore, in the following s_0 is replaced by μ.

As discussed in Ref. [22] Eq. (11) can be considered to describe an evolution process, similar to the Lipatov-Altarelli-Parisi (LAP) equation. $A(s/s_i,\kappa)$ represents the upper part of the ladder in Fig. 1 down to the subenergy

$$s_i = \beta_i\,(1+\alpha_i)\,s\ . \tag{13}$$

The subsequent decrease from s_i to s_{i+1} may induce the emission of the next s-channel gluon. This situation is described by the first term of Eq. (11). The second term gives the probability that no s-channel gluon is emitted:

$$w(s_i,s_{i+1}) = \exp\left(-2\alpha(\kappa_i)\ln\frac{s_i}{s_{i+1}}\right)\ . \tag{14}$$

Based on this observation the simulation procedure for creating the multigluon state can be constructed. Starting with $s_1 = s$ one samples the new subenergy according to the "decay probability" (14). If $s_{i+1} \le \mu^2$ the iteration stops. Otherwise the new transverse momentum κ_{i+1} has to be sampled from Eq. (11). In order to do that the following substitution is introduced:

$$A(s,\kappa) = \left(\frac{s}{\mu^2}\right)^{2\alpha(\kappa)}\tilde{A}(s,\kappa). \tag{15}$$

Together with Eq. (11) we get

$$\frac{d}{d\ln\mu^2/s}\tilde{A}(s,\kappa) = \frac{2g^2N}{(2\pi)^3}\kappa^2\int\frac{d^2\kappa'}{\kappa'^2|\kappa-\kappa'|^2}\left(\frac{s}{\mu^2}\right)^{2[\alpha(\kappa')-\alpha(\kappa)]}\tilde{A}(s,\kappa')\ . \tag{16}$$

Therefore, the new transverse momentum κ_{i+1} has to be chosen from the distribution

$$\frac{\kappa_i^2 d^2\kappa_{i+1}}{\kappa_{i+1}^2|\kappa_i-\kappa_{i+1}|^2}\theta\left(\kappa_{i+1}-\mu\right)\theta\left(|\kappa_i-\kappa_{i+1}|-\mu\right)\left(\frac{s_{i+1}}{\mu^2}\right)^{2[\alpha(\kappa_{i+1})-\alpha(\kappa_i)]} \tag{17}$$

Assigning a mass m to the produced s-channel gluon, the kinematics of the considered branching is fixed completely. For simplicity and in order to avoid additional free parameters we set $m = 0$. Note, that the last s-dependent factor of Eq. (17) is not taken into account in Ref. [22]. However, this factor is of great importance to reproduce the hardening of the intermediate multigluon state with increasing energy (see Sec. IV).

B. The coupling to the hadron

Now I discuss the coupling of the PP to the incoming hadrons. The amplitude $\mathcal{A}(s,q,\kappa)$ describes the properties of the PP. In order to obtain the "physical" elastic amplitude for the process $h_1h_2 \to h_1h_2$, $\mathcal{A}(s,q,\kappa)$ has to be convoluted with the PP-hadron couplings (depending on κ) which cannot be calculated from PQCD. From Regge arguments it should be expected that this convolution would not introduce additional energy dependence. Thus, the total hadron-hadron cross section should behave at high energies like

$$\sigma_{\rm tot} \sim s^{\Delta},\quad \Delta \sim 0.5 \tag{18}$$

[see Eq. (7)]. However, phenomenologically hadronic cross sections rising like

$$s^{\epsilon},\quad \epsilon \sim 0.08 \tag{19}$$

are observed, ϵ being nearly constant up to $\sqrt{s} = 1.8$ TeV (see the next section). Therefore, it may be concluded that next-to-leading contributions to the PP may be important in order to obtain the right asymptotic behavior of the total cross sections [26]. In the present paper, I assume that the QCD ladder does not couple to the incoming hadrons as a whole, but instead this coupling is determined by the coupling of the first t-channel Reggeized gluon. It will be shown in the following that with this assumption the intercept of the Pomeron can be expressed through the intercept of this Reggeized gluon given in Eq. (1).

We are interested in the total cross section for the collision of two hadrons h_1, h_2 with four-momenta p_1 and p_2, $(p_1+p_2)^2 = s$. Let us consider partons from h_1 and h_2 with $p_1' = x_1p_1 + \kappa$ and $p_2' = x_2p_2 + \kappa$, respectively. Up to now we have considered the evolution of the QCD ladder in the case, where in every step an s-channel gluon with a transverse momentum larger than μ is emitted. However, there is the possibility that in the first step of the evolution the new subenergy chosen from Eq. (14) is below μ^2. In this case, the considered gluon

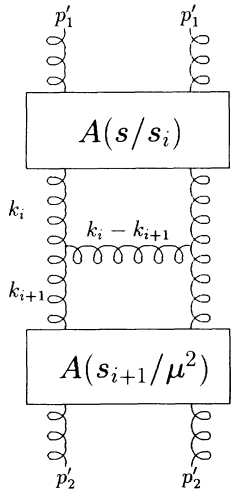

FIG. 1. Graphical representation of Eq. (11).

p_1' evolves from $s_1 = x_1 x_2 s$ down to μ^2 with no s-channel gluon emission with a transverse momentum larger than μ. The imaginary part of the forward amplitude for this "pure soft" interaction will be denoted by $A_s(x_1 x_2 s, \kappa)$. According to Eq. (14) the probability for this "pure soft" situation is

$$w_0 = \exp\left(-2\alpha(\kappa)\ln\frac{x_1 x_2 s}{\mu^2}\right) = \left(\frac{x_1 x_2 s}{\mu^2}\right)^{-2\alpha(\kappa)} . \tag{20}$$

On the other hand this probability is given by the ratio of the "soft" divided by the total cross section:

$$w_0 = \frac{A_s(x_1 x_2 s, \kappa)}{A_s(x_1 x_2 s, \kappa) + A(x_1 x_2 s, \kappa)} = \frac{A_s(x_1 x_2 s, \kappa)}{A_{\rm tot}(x_1 x_2 s, \kappa)} . \tag{21}$$

In the above expression, the "total" amplitude $A_{\rm tot}$ was introduced, containing the perturbative and soft contributions. Combining (20) and (21) and summing over all possible energy fractions and virtualities of the initial gluons we obtain the total cross section for the interaction of the two hadrons via the exchange of a QCD ladder with inclusion of the soft contributions:

$$\sigma_{\rm tot} = \int dx_1 dx_2 d^2\kappa G_1(x_1,\kappa) G_2(x_2,\kappa) \left(\frac{x_1 x_2 s}{\mu^2}\right)^{2\alpha(\kappa)} A_s(x_1 x_2 s, \kappa) . \tag{22}$$

The functions $G_i(x,\kappa)$ describe the properties of the hadron h_i and has to vanish rapidly for $\kappa \geq \mu$. On the other hand $\alpha(\kappa)$ becomes a constant for large κ. It can be expected that A_s, representing the soft part of the interaction would not be an increasing function of κ. Therefore, the κ integration can be replaced by the value of the integrand at some average value κ_0 with $\kappa_0 \sim \mu$:

$$\sigma = \left(\frac{s}{\mu^2}\right)^{2\alpha(\kappa_0)} \int dx_1 dx_2 F_1(x_1) F_2(x_2) A_s(x_1 x_2 s, \kappa_0) = \sigma_0 \left(\frac{s}{\mu^2}\right)^{2\alpha(\kappa_0)} . \tag{23}$$

In the above expression, I have introduced

$$F_i(x_i) = x_i^{2\alpha(\kappa_0)} G_i(x_i, \kappa_0) . \tag{24}$$

σ_0 is the cross section for the interaction with no minijet production (Fig. 2) and will be assumed to be energy independent. The energy dependence of the total cross section is simply determined by the intercept of the Reggeized gluon, calculated at κ_0 with a regularization cutoff μ. The object described by Eq. (23) and including the contributions from both the perturbative Pomeron and the "pure soft" interaction will be called in the following a Pomeron.

Let me now summarize the results of this section. Based on the results of Ref. [22] an evolution procedure for the multigluon intermediate state of the PP is constructed. Making some very simple and rather general assumptions on the structure of a hadron, a formula is found, describing the total cross section for high energy hadron-hadron collisions given by Pomeron exchange and the relative weight of the soft part as compared to the perturbative part of the interaction. The free parameter κ_0 will be fixed in the next section.

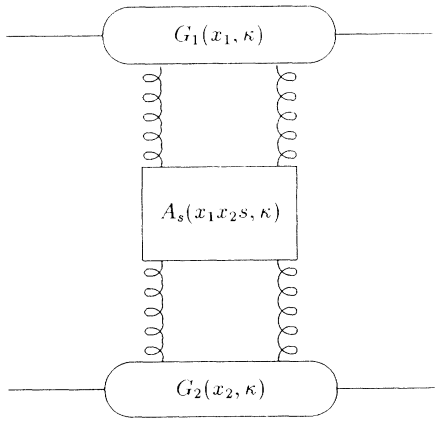

FIG. 2. The "pure soft" interaction.

III. CROSS SECTIONS

As shown by Donnachie and Landshoff [27,28] a simple Regge fit of the form

$$\sigma_{\rm tot} = X s^{\epsilon} + Y s^{\eta} \tag{25}$$

gives a very good description of all available experimental data on hadronic total cross sections. In the above expression, the first term arises from Pomeron exchange and the second from ρ, ω, f, a exchange. ϵ and η are related to the value of the Pomeron and Reggeon trajectories $\alpha_P(q^2)$ and $\alpha_R(q^2)$ for $q^2 = 0$:

$$\epsilon = \alpha_P(0) - 1, \quad \eta = \alpha_R(0) - 1. \tag{26}$$

In Ref. [28] it was found that the best fit is obtained for

$$\epsilon = 0.0808, \quad \eta = -0.4525. \tag{27}$$

As shown in the previous section the intercept of the Pomeron can be expressed through the intercept of the Reggeized gluon:

$$\alpha_P(0) = 1 + 2\alpha(\kappa_0). \tag{28}$$

It can be easily checked by numerical integration of Eq. (1) with condition (12) that for any reasonable value of the regularization parameter μ and the QCD scale Λ, a parameter value κ_0 of order μ can be found with

$$2\alpha(\kappa_0) = \epsilon. \tag{29}$$

It has been discussed in [28] that ϵ is an effective power also including effects from multi-Pomeron exchange. These multiple exchanges reduce ϵ with increasing energy, but the data indicate that the variation of ϵ with the energy is rather small. Furthermore, it was pointed out by Collins and Gault [29], that an almost constant power causes no problems with the Froissart-Martin bound, because at present energies that bound is about 10 b, way above the data. However, while studying particle production, I have found that it is in principle possible to describe some of the experimental data, such as the average charged particle multiplicity and the rise of the pseudorapidity plateau height within a model with single Pomeron exchange. But it turns out that multiplicity fluctuations and two-particle correlations cannot be satisfactorily reproduced [23]. Thus, although corrections to the total cross section due to multiple Pomeron exchange may be small, they are important when we consider multiparticle production in high energy hadron-hadron collisions. Indeed, it would be very nice if we were able to take unitarity corrections from PQCD directly but at present we cannot do that. Therefore some additional assumptions are necessary to account for the effects of multiple Pomeron exchange and to calculate the relative weight for an n-Pomeron graph.

We consider the single Pomeron amplitude for the interaction $h_1h_2 \to h_1h_2$:

$$A_1(s,t) = g_1(t)g_2(t)\exp\left[\xi \cdot \alpha_P(t)\right] \tag{30}$$

with $\xi = \ln(s/\mu^2) - i\pi/2$. Because we are interested in calculating total and elastic cross sections, it is sufficient to consider a linear Pomeron trajectory and exponential couplings:

$$\begin{aligned} \alpha_P(t) &= \alpha_P(0) + \alpha'_P t = 1 + 2\alpha(\kappa_0) + \alpha'_P t, \\ g_i(t) &= g_i(0)\exp(b_i t), \quad g_1(0)g_2(0) = \sigma_0. \end{aligned} \tag{31}$$

Let me now introduce the impact parameter representation of (30):

$$\chi_P(s,b) = \frac{i}{4\pi s}\int_{-\infty}^{0} dt J_0(b\sqrt{-t})A_1(s,t) = \frac{\sigma_0}{8\pi b_P}\exp\left(-\frac{b^2}{4b_P} + 2\alpha(\kappa_0)\cdot\xi\right), \tag{32}$$

where $b_P = b_P^{(0)} + \alpha'_P\xi$, $b_P^{(0)} = b_1 + b_2$. If we approximate the n-Pomeron-hadron coupling by the product of the n single Pomeron-hadron couplings,

$$G_n(t_1, t_2, \ldots, t_n) = \prod_{i=1}^{n} g(t_i), \tag{33}$$

we obtain, for the n-Pomeron amplitude (Fig. 3) [30],

$$A_n(s,t) = \frac{4\pi s}{in!}\int_0^\infty b db J_0(b\sqrt{-t})\left[-\chi_P(s,b)\right]^n. \tag{34}$$

Summing over all n we get the elastic h_1h_2 scattering amplitude in the eikonal form

$$A(s,t) = \sum_{n=1}^{\infty} A_n(s,t) = 8\pi s\int_0^\infty b db J_0(b\sqrt{-t})\frac{\exp\left[-\chi_P(s,b)\right] - 1}{2i}. \tag{35}$$

[We use the normalization $\sigma_{\text{tot}} = \text{Im}A(s,t=0)/s$.] Equation (35) can be simply generalized to the case, when we consider more than one Reggeon. The only difference is that χ_P has to be replaced by the sum of the different Reggeon amplitudes.

The experimental data are most extensive for pp and $p\bar{p}$ collisions. Because we are interested in describing particle production in the collider energy range, it is in principle sufficient to consider only Pomeron exchange. However, as pointed out in [28], the constraint on the Pomeron intercept is much stronger due to the data in the energy range from $\sqrt{s} = 10$ GeV to CERN Intersecting Storage Rings (ISR) energy, where the contribution from ρ, ω, f, a exchange, although small as compared to the Pomeron, cannot be neglected. We take this contribution into account by an effective trajectory $\alpha_R(t) = \alpha_R(0) + \alpha'_R t$:

$$\chi_R^{(i)}(b,s) = \frac{\sigma_R^{(i)}}{8\pi b_R^{(i)}}\exp\left(-\frac{b^2}{4b_R^{(i)}} + \alpha_R(0)\xi^{(i)}\right), \quad i = 1,2,$$

$$\chi_R(b,s) = \chi_R^{(1)}(b,s) + \chi_R^{(2)}(b,s) \quad \text{for} \quad p\bar{p},$$

$$\chi_R(b,s) = \chi_R^{(1)}(b,s) - \chi_R^{(2)}(b,s) \quad \text{for} \quad pp, \tag{36}$$

where $\xi^{(1),(2)} = \ln(s/\mu^2) \mp i\pi/2$. The Reggeon slopes are

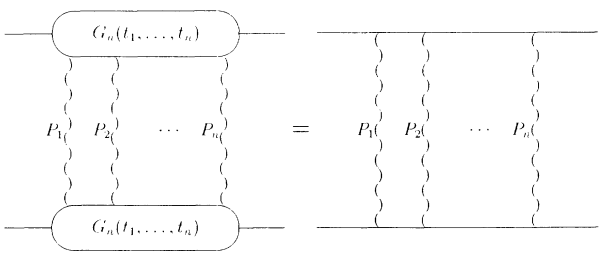

FIG. 3. The n-Pomeron amplitude.

TABLE I. Pomeron parameters as obtained from the fit to the total and elastic cross sections.

$\alpha_P(0)$	$\alpha_P'^{\star}$ (GeV^{-2})	σ_0 (mb)	$b_P^{(0)}$ (GeV^{-2})
1.0922	0.25	24.86	3.26

given as in the Pomeron case by $b_R^{(i)} = b_R^{(0)(i)} + \alpha_R' \xi^{(i)}$.

The model parameters are fixed by simultaneously fitting the experimental data [31] on the total and elastic cross sections $\sigma_{\rm tot}$ and $\sigma_{\rm el}$:

$$\sigma_{\rm tot} = 8\pi \int_0^\infty bdb \ {\rm Im} \ \frac{\exp\left[-\chi_P(s,b) - \chi_R(s,b)\right] - 1}{2i},$$

$$\sigma_{\rm el} = 8\pi \int_0^\infty bdb \left| \frac{\exp\left[-\chi_P(s,b) - \chi_R(s,b)\right] - 1}{2i} \right|^2, \quad (37)$$

in the energy range 10 GeV $\leq \sqrt{s} \leq$ 1800 GeV and are summarized in Tables I and II. The parameter denoted with a star was not included in the fitting procedure. In Figs. 4–6, $\sigma_{\rm tot}, \sigma_{\rm el}$, and $\rho = {\rm Im}A(s,t=0)/{\rm Re}A(s,t=0)$ are compared with the experimental data. The agreement is excellent, as already indicated by the $\chi^2/N_{\rm DF} = 1.05$.

In conclusion of this section let me make some comments.

(1) The "bare" Pomeron intercept was found to be $2\alpha(\kappa_0) = 0.0922$. This value is not far from the effective power discussed in the beginning of this section. Moreover, if we define

$$\Delta_{\rm eff} = \frac{1}{\sigma_{\rm tot}} \frac{d\sigma_{\rm tot}}{d\ln s}, \quad (38)$$

$\Delta_{\rm eff}$ is almost equal to ϵ.

(2) Although an eikonal formula for the elastic scattering amplitude is used, I want to emphasize that the presented model is not a geometrical one. The rise of the cross sections does not reflect the fact that hadrons become "bigger" and "blacker," but represents the properties of what is exchanged, the Pomeron. In this model the Pomeron properties are expressed through the properties of the Reggeized gluon, a general and interaction independent object. Thus, the experimentally observed universal rise of hadronic total cross sections can be explained by the model.

(3) The precise value of α_P' cannot be fixed in a unique manner from the pp and $p\bar{p}$ total and elastic cross sections. We have used the usual value $\alpha_P' = 0.25$ GeV^{-2}. With this, we predict $\sigma_{\rm tot} = 113$ mb at the Superconducting Super Collider (SSC) energy. However, changing α_P' in the range 0.2–0.3 GeV^{-2}, the fit quality remains almost unchanged, while the total cross section at SSC energy varies from 110 mb to 117 mb.

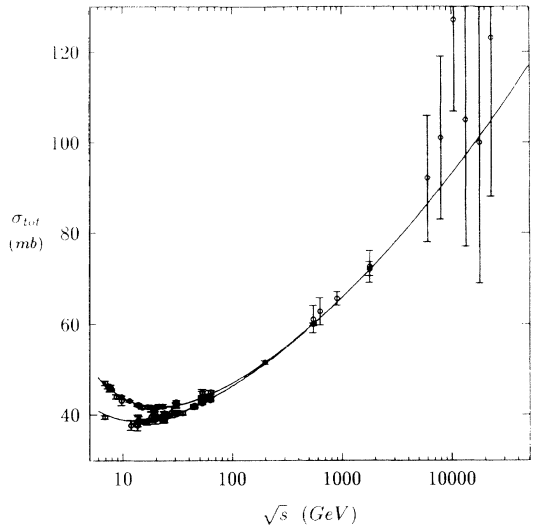

FIG. 4. The fit on the total cross section $\sigma_{\rm tot}$ as compared with experimental data.

IV. PARTICLE PRODUCTION

The inelastic cross section is given by the absorptive part of the elastic scattering amplitude. The absorptive part of the single Pomeron amplitude will be called as usual a cut Pomeron. In Fig. 7 we show the different contributions to a single cut Pomeron. The first term on the right-hand side of Fig. 3 represents the "pure soft" interaction, the sum over all other graphs is equal to the absorptive part of the PP amplitude convoluted with $G_1(x_1,\kappa_0)G_2(x_2,\kappa_0)$. From the Abramovski-Gribov-Kancheli (AGK) cutting rules [32] and Eq. (34) the topological cross sections for having n-cut Pomerons can be calculated:

$$\sigma_n = 2\pi \int_0^\infty bdb \frac{\left[2\chi^R(s,b)\right]^n}{n!} \exp\left[-2\chi^R(s,b)\right]. \quad (39)$$

Here (and in the following), the Reggeon contribution was neglected for simplicity because the cross section to have a cut Reggeon is below 1% in the collider energy range. The generalization of (39) to the case of different Reggeon trajectories is straightforward. In Eq. (39) $\chi^R = {\rm Re}(\chi_P)$. Note that

$$\sum_{n=1}^{\infty} \sigma_n = \sigma_{\rm in} = \sigma_{\rm tot} - \sigma_{\rm el}. \quad (40)$$

When we consider n-cut Pomerons, we have to specify the momentum fractions x_i, y_i of the n gluons from the projectile and from the target with the virtualness κ_0 between which the Pomerons are exchanged. As has been

TABLE II. Reggeon parameters as obtained from the fit to the total and elastic cross sections.

$\alpha_R(0)^{\star}$	$\alpha_R'^{\star}$ (GeV^{-2})	$\sigma_R^{(1)}$ (mb)	$b_R^{(0),(1)}$ (GeV^{-2})	$\sigma_R^{(2)}$ (mb)	$b_R^{(0),(2)}$ (GeV^{-2})
0.56	0.8	144.5	2.30	28.1	22.18

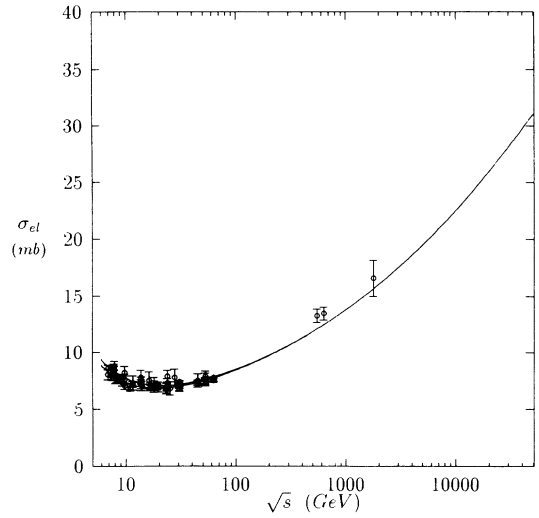

FIG. 5. The fit on the elastic cross section $\sigma_{\rm el}$ as compared with experimental data.

discussed in Sec. II, in the one Pomeron case, the x distribution of the gluons is given by $F(x)$. We want to assume that the n-gluon distribution function F_n is

$$F_n(x_1,\ldots,x_n) = \theta\left(1-\sum_{i=1}^{n} x_i\right)\prod_{i=1}^{n} F(x_i). \tag{41}$$

It remains to specify $F(x)$. In some sense, the situation here is similar to the case when the LAP equations are used to evaluate the hadron structure function. There, one needs a starting distribution $f(x,Q_0^2)\sim(1-x)^a/x^J$. Therefore, I have fixed

$$F(x) = C(1-x)^a, \tag{42}$$

C being a normalization constant. The $1/x^J$ behavior for small x values is then obtained through the evolution of the PP ladder.

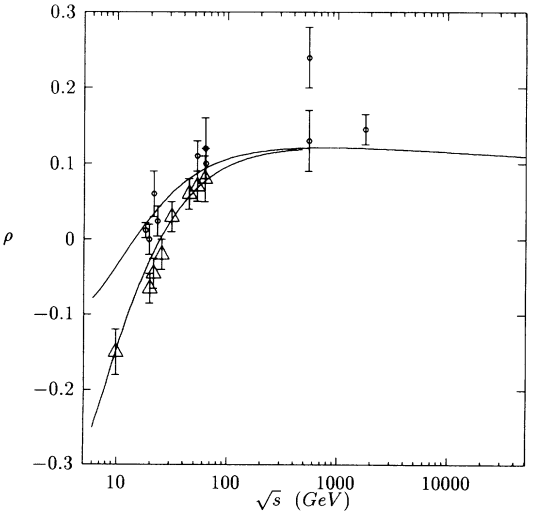

FIG. 6. The resulting ratio of the real to the imaginary part of the forward elastic scattering amplitude compared to experimental data.

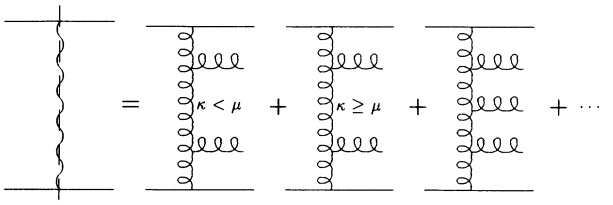

FIG. 7. The contributions to the cut Pomeron.

Equations (39) and (40) determine the probability to have an event with n-cut Pomerons. Equations (41) and (42) describe the distribution function of the gluons which initiate the PP-ladder evolution. Therefore, together with the simulation procedure discussed in Sec. II, the s-channel multigluon intermediate state of the Pomeron is completely specified. As a first check of the model, the transverse momentum distribution of the gluons in $|\eta|<1.5$ in $p\bar{p}$ collisions at $\sqrt{s}=200$ and 900 GeV was calculated and is compared in Fig. 8 with the minijet cross section measured by the UA1 Collaboration [33]. The agreement is very good. Here and in the following, the values of μ, Λ, and a were fixed to

$$\begin{aligned}&\mu = 1 \text{ GeV},\\ &\Lambda = 0.25 \text{ GeV},\\ &a = 5.\end{aligned} \tag{43}$$

Let me now discuss the hadronization of the Pomeron intermediate state. The gluons are splitted into a $q\bar{q}$ pair according to the Altareli-Parisi splitting functions

$$P_{Gq}(z) = \frac{3}{2}\left[z^2+(1-z)^2\right]. \tag{44}$$

For the splitting of the valence remnants Regge arguments are used again. This implies for a valence quark (or antiquark),

$$P_q^B(z) = \frac{(1-z)^{3/2}}{\sqrt{z}} \tag{45}$$

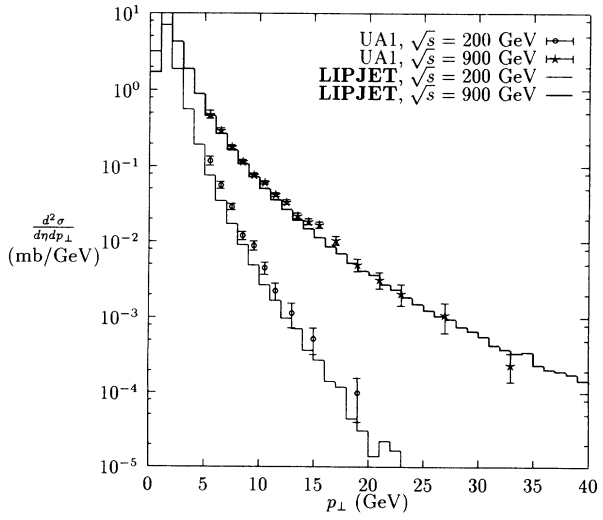

FIG. 8. Invariant minijet cross section in $|\eta|\leq 1.5$ calculated by LIPJET (histograms) and compared to UA1 data [33].

in the case of a baryon, and

$$P_q^M(z) = \frac{1}{\sqrt{z}\sqrt{1-z}} \tag{46}$$

in the case of a meson [21]. Then a color configuration is chosen randomly and $q-\bar{q}, q-qq, \bar{q}-\bar{q}\bar{q}, qq-\bar{q}\bar{q}$ color singlets are formed. The resulting "strings" or "chains" are converted into hadrons by the fragmentation code BAMJET [34, 35] or optionally JETSET 7.3 [36, 37].

V. RESULTS

In this section I study particle production in $p\bar{p}$ collisions in a wide energy range, from $\sqrt{s}$ = 50 GeV up to Fermilab Tevatron energy $\sqrt{s}$ = 1800 GeV with the Monte Carlo implementation of the presented model, the code LIPJET. Note that, in addition to the parameters describing the fragmentation of the strings, the only free parameters are given in (43). The initial virtualness κ_0 and the probability distribution for having an n-cut Pomeron event are fixed from the fit on the total and elastic cross sections. In all calculations the fragmentation code BAMJET with the same set of parameters is used. I have checked that there is no significant difference in the results when the code JETSET with default settings is used, except in the transverse momentum distribution of high $p_\perp$ charged hadrons. This difference arises from the different fragmentation functions of both models (see Sec. V C). Because in the present version of the model diffractive excitations are not taken into account, in the following all results calculated by the model are compared with measurements in non-single-diffractive events.

A. Charged multiplicity and multiplicity distributions

In Fig. 9 the average charged multiplicity $\langle N_c \rangle$ as calculated by LIPJET is compared with experimental results from the ISR [38], UA5 [39, 40], and E735 [41] collaborations. The energy dependence of $\langle N_c \rangle$ is reproduced very good. In Fig. 10 the charged particle multiplicity distributions at $\sqrt{s}$ = 200 and 900 GeV as measured by the UA5 [39] are found to be in good agreement with the results of the model. In order to show the violation of KNO scaling, the energy dependence of the normalized moments of the distributions

$$C_q = \frac{\langle N_c^q \rangle}{\langle N_c \rangle^q} \tag{47}$$

are plotted in Fig. 11, together with experimental data.

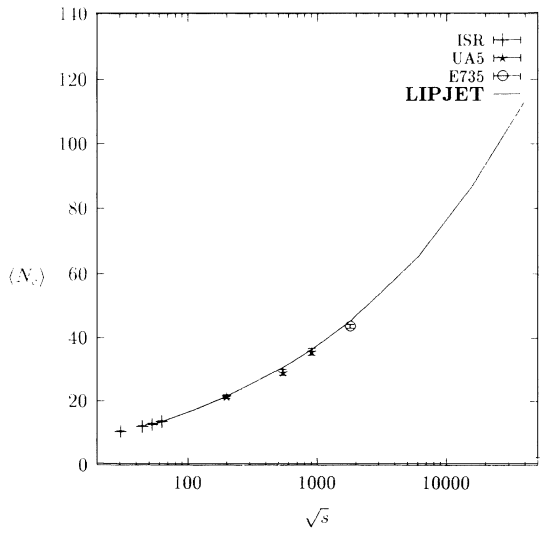

FIG. 9. Average charged multiplicity in $p\bar{p}$ collisions as calculated by LIPJET (line) and compared to ISR, UA5, and E735 data [38–41].

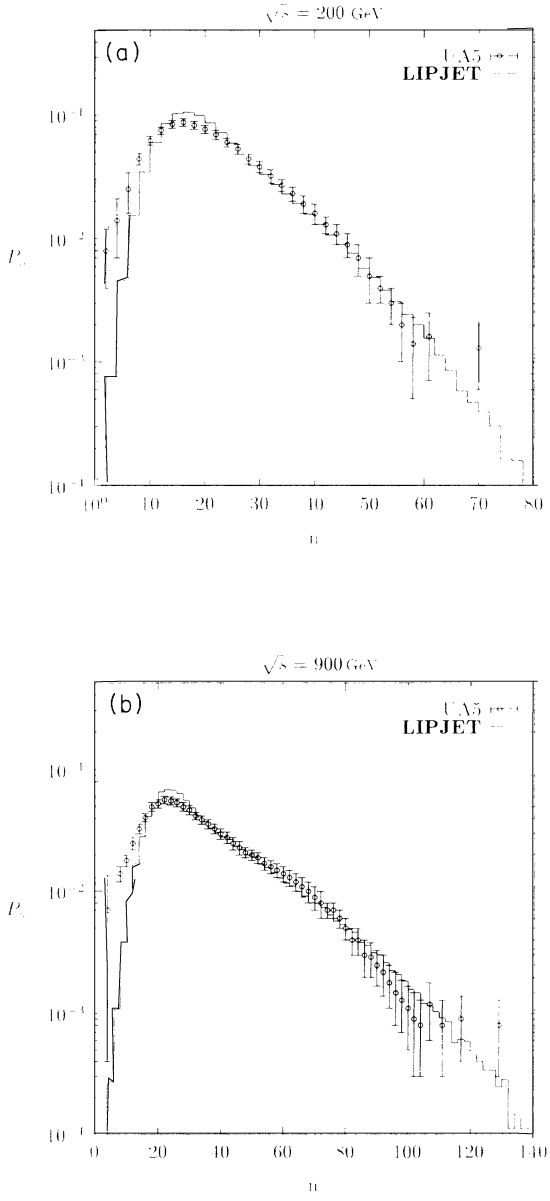

FIG. 10. The charged multiplicity distribution in $p\bar{p}$ collisions from our model (histogram) and from the UA5 data (points): (a) $\sqrt{s}$ = 200 GeV, (b) $\sqrt{s}$ = 900 GeV. The data are from Ref. [39].

B. Rapidity distributions

The rapidity y and pseudorapidity η of a particle are defined by

$$y = \frac{1}{2} \ln \frac{E + p_L}{E - p_l},$$

$$\eta = \frac{1}{2} \ln \frac{p + p_L}{p - p_l},$$

with p_L the momentum component in beam direction. In Fig. 12 the pseudorapidity distributions of charged particles calculated by LIPJET at $\sqrt{s} = 53$, 200, 546 and 1800 GeV are shown to be in good agreement with the UA5 [42], and Collider Detector at Fermilab (CDF) [43] data. Both, the overall widening of the distributions and the increase of the central pseudorapidity density $\rho(0)$ are well reproduced. In Fig. 13 I show the rise of $\rho(0)$ with the energy together with UA1 [44], UA5 [42] and CDF [43] data.

In [22] it was found that the hadronic intermediate state of a single Pomeron shows an energy-independent middrapidity density. This is indeed due to the fact

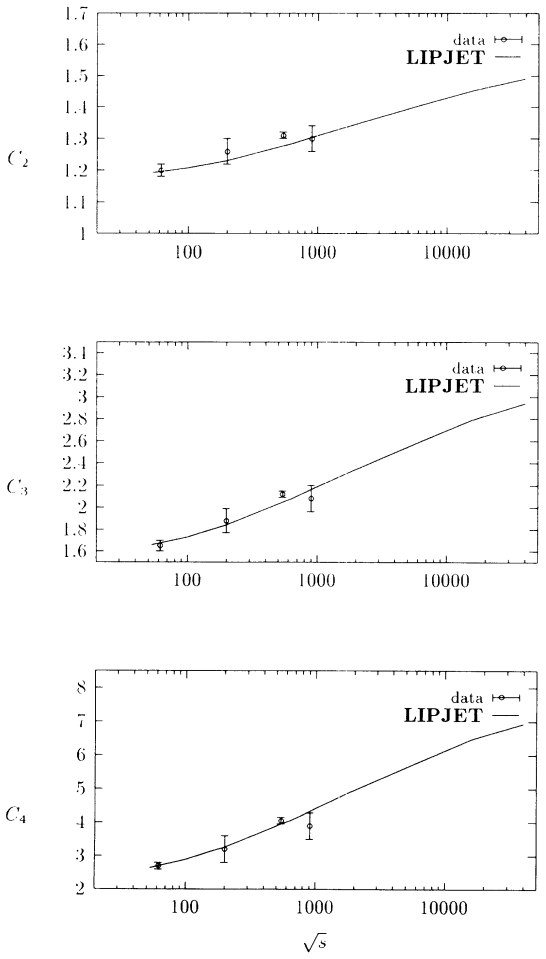

FIG. 11. The increase of the moments of the multiplicity distribution with the energy. The experimental data are from Refs. [39, 40].

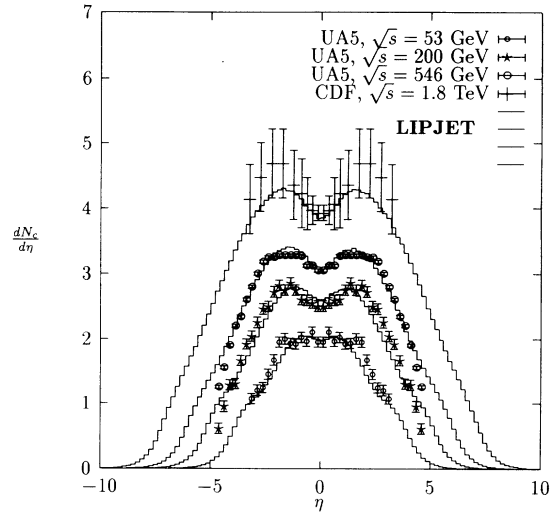

FIG. 12. Charged particle pseudorapidity distribution from the LIPJET calculation together with UA5 [42] and CDF [43] data.

that in the model of Ref. [22] the gluons (having a fix mass of $m = 10$ GeV) are converted independently from each other into hadrons, violating in this manner the color conservation. In my model, the hadrons coming from one-cut Pomeron show rising with energy rapidity plateau. We have in the average 1.5-cut Pomerons at $\sqrt{s} = 50$ GeV and 2.3-cut Pomerons at $\sqrt{s} = 40$ TeV, while $\rho(0)$ grows from ~ 2 to ~ 7.9. This corresponds to a pseudorapidity density per cut Pomeron of about 1.33 at $\sqrt{s} = 50$ GeV and 3.41 at the SSC energy. Moreover, if we consider a model with a single Pomeron exchange and assume that partons with the maximal distance in phase space form the colorless strings, it is possible to reproduce the observed rise of $\rho(0)$ with the energy [23].

By the UA7 Collaboration was measured the π^0 rapidity distribution in the fragmentation region at $\sqrt{s} =$

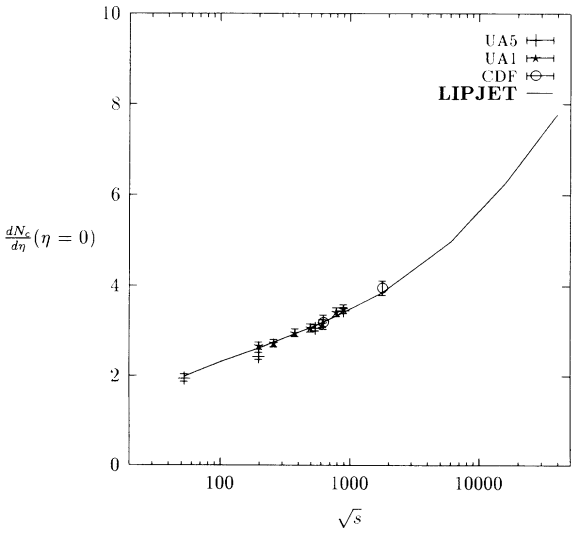

FIG. 13. The rise of the pseudorapidity density at $\eta = 0$. Data are from [42–44] data.

630 GeV [45]. The UA7 results are shown to be described well by LIPJET in Fig. 14.

C. Transverse flow

There are two sources for transverse momenta in the presented model.

(1) The transverse momenta from the string fragmentation. In the fragmentation code BAMJET they are chosen from the distribution

$$\frac{dN}{p_\perp dp_\perp} = C\exp(-b\sqrt{p_\perp^2 + m^2}), \tag{48}$$

with C a normalization constant, m the particle mass, and $b = 8\ \mathrm{GeV}^{-1}$.

(2) The transverse momenta of the s-channel gluons of the Pomeron. For $p_\perp > \mu$ the transverse momentum distribution of these gluons is described by PQCD via the equation of the PP [(11) and (17)]. In the case $p_\perp < \mu$ (this is the case when in the first step of the ladder evolution the new subenergy is below μ^2) the $p_\perp$ is chosen from a uniform distribution in the range $0 \le p_\perp \le \mu$.

Shown in Fig. 15 are the inclusive invariant cross sections for charged particle production as a function of $p_\perp$ from the LIPJET calculation as compared to the experimental data at $\sqrt{s} = 200$ and 900 GeV [44]. The agreement is good. The light overprediction of LIPJET for $p_\perp \ge 4$ GeV can be explained as follows: We assume for simplicity that high $p_\perp$ hadrons come from the first step of the hadronization of a string and carry a fraction z of the momentum of the string end. If we then neglect the hadron mass and the additional transverse momentum from the fragmentation, we can write

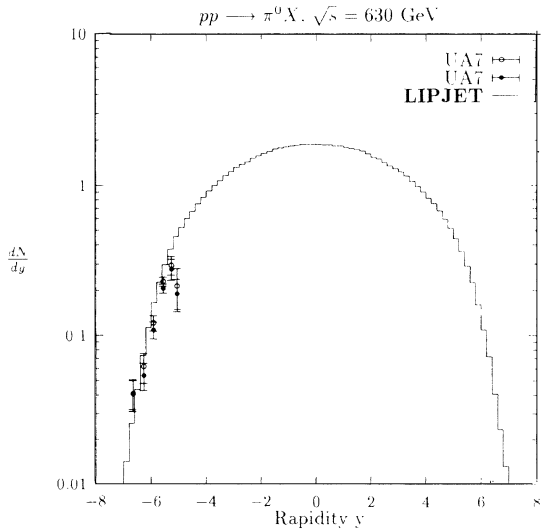

FIG. 14. Comparison of the rapidity distribution of π^0 at $\sqrt{s} = 630$ GeV in the fragmentation region. The data are from Ref. [45], the histogram is the LIPJET result.

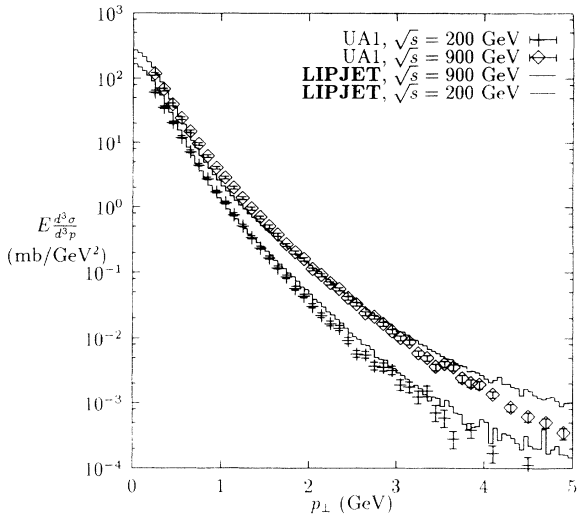

FIG. 15. Invariant cross section for the production of a charged hadron in $|\eta| \le 2.5$ as a function of the transverse momentum. The points represent the UA1 results [44], the histogram the LIPJET calculation.

$$\frac{d^2N_h}{p_\perp dp_\perp dy} \sim \int p'_\perp dp'_\perp \frac{d^2N_p}{p'_\perp dp'_\perp dy} f(z)dz\delta(p_\perp - zp'_\perp)$$
$$= \int dp'_\perp \frac{d^2N_p}{p'_\perp dp'_\perp dy} f\left(\frac{p_\perp}{p'_\perp}\right). \tag{49}$$

Here, $f(z)$ denotes the fragmentation function, the subscript h stands for "hadron" and p for "parton." From the above expression it is clear that the precise shape of the $p_\perp$ distribution in LIPJET depends on the fragmentation function $f(z)$. Remember that the $p_\perp$ dependence of the minijet cross section is reproduced very well by the model (Fig 8). Indeed, I have checked that it is possible to better reproduce the experimental data, if different parameters in the hadronization of chains with transverse momenta of the chain ends larger than μ are used. However, because I am interested in having a model with a minimum of assumptions and free parameters, for all strings the same default set is used.

D. Kaon production

In Fig. 16 the transverse momentum distribution of kaons at two different energies as calculated by LIPJET is compared with the results from the UA5 Collaboration [46]. The agreement is excellent. In Fig. 17 the K rapidity distribution is shown together with the experimental data. The increase and widening of the distribution with the energy is reproduced. It seems that LIPJET slightly overestimates the kaon rate. Note, that the number of K mainly depends on the parameters of the hadronization. In all calculations, the BAMJET parameters as fixed from e^+e^- data are used. I have checked that with a small modification of the parameter describing the probability to produce a given q flavor, the K production rate can be better described. In Fig. 18 the K/π ratio is plotted as a function of the transverse momentum together with UA5 data [47].

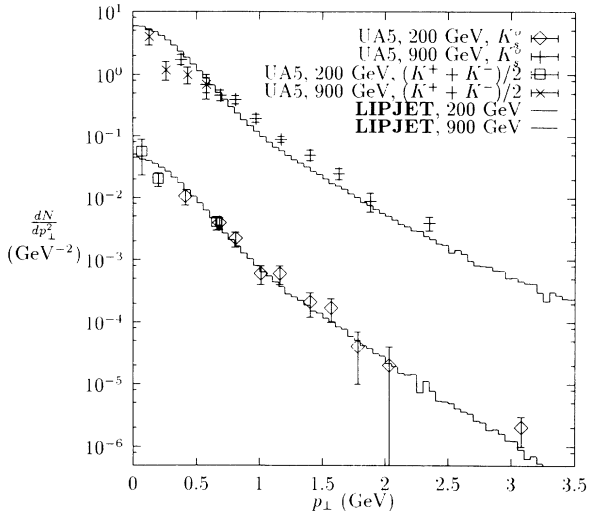

FIG. 16. Transverse momentum distribution of kaons in $|y| \leq 2.5$ measured by the UA5 Collaboration [46] together with our results (histogram).

E. Particle correlations

The study of the correlations between the final state particles are important in order to reveal the properties of the underlying production mechanism in more detail. First, we consider two-particle correlation in rapidity. The most common models to explain the observed two-particle correlations are cluster models [48, 49], in which the final state particles are created from the isotropic decay of the clusters. From a general point of view, the fragmentation of minijets can be considered as the decay of clusters with a constant width in rapidity, as found in the experimental study of jet profiles [33].

The two-particle correlation in the pseudorapidity is defined as

$$C(\eta_1, \eta_2) = \rho(\eta_1, \eta_2) - \rho(\eta_1)\rho(\eta_2) \ , \tag{50}$$

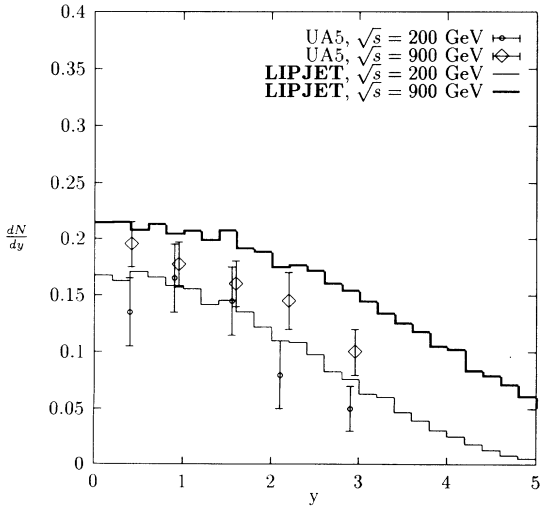

FIG. 17. Rapidity distribution of kaons as calculated by LIPJET together with the measurement by the UA5 Collaboration [46].

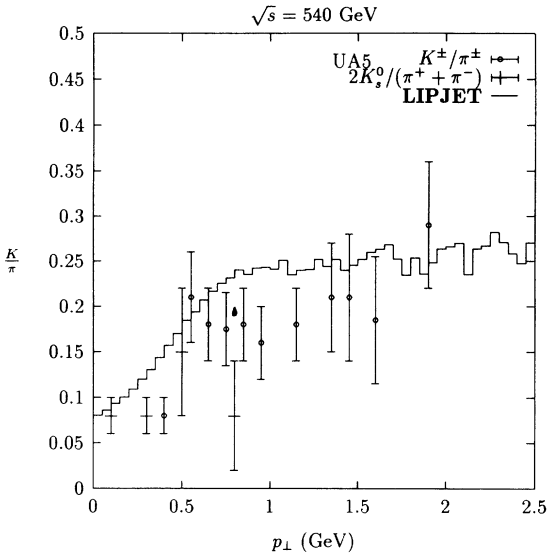

FIG. 18. K/π ratio as a function of the transverse momentum at $\sqrt{s} = 546$ GeV. Data are from [47].

where $\rho(\eta_1, \eta_2)$ is the two-particle density which is proportional to the probability of joint particle production at η_1 and η_2. Similarly one can define the semi-inclusive two-particle correlation function $C_n(\eta_1, \eta_2)$ for events with a fixed multiplicity n. An intrinsic correlation function $C_s(\eta_1, \eta_2)$ can be expressed in terms of $C_n(\eta_1, \eta_2)$ as

$$C_s(\eta_1, \eta_2) = \sum_n P_n C_n(\eta_1, \eta_2) \tag{51}$$

with P_n the probability to find an event with the multiplicity n. $C_s(\eta_1, \eta_2)$ is usually referred to as a "short range" correlation function, because as we will see below that is sharply peaked at $\eta_1 = \eta_2$.

In Fig. 19, our calculated $C(0, \eta)$ is plotted together with the UA5 data [50] at $\sqrt{s} = 200$ and 900 GeV. The

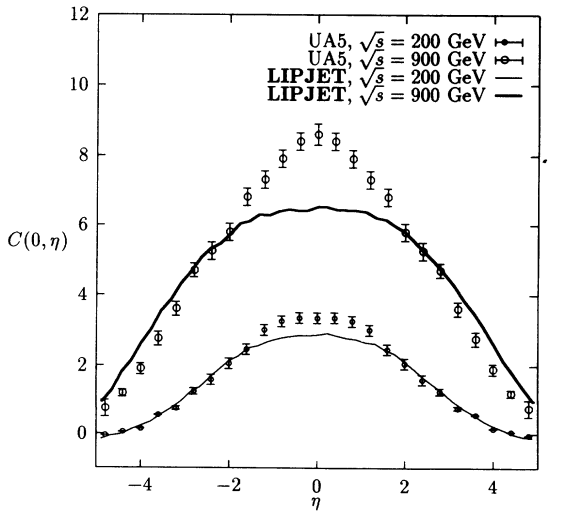

FIG. 19. The two-particle correlation function $C(0, \eta)$ at $\sqrt{s} = 200$ and 900 GeV. The lines correspond to the LIPJET calculation, the points to the UA5 data [50].

about 25% underprediction of LIPJET at $\eta = 0$ is not understood at present. Note, that in the model HIJING a similar underprediction is observed [8]. In Fig. 20 $C_s(0,\eta)$ is compared to the experimental data [50]. The qualitative shape of the "short range" correlation is reproduced by LIPJET.

The long range forward-backward correlation can be studied by looking at particle production in two rapidity bins with the size $\delta\eta$ separated by a rapidity gap $\Delta\eta$. Let me denote the number of particles with rapidities between $\Delta\eta/2$ and $\Delta\eta/2 + \delta\eta$ as n_F and those between $-\Delta\eta/2$ and $-\Delta\eta/2-\delta\eta$ as n_B. For a system with $\langle n_F\rangle = \langle n_B\rangle$ and $\langle n_F^2\rangle = \langle n_B^2\rangle$, the forward-backward correlation strength is defined by

$$b = \frac{\langle n_F n_B\rangle - \langle n_F\rangle^2}{\langle n_F^2\rangle - \langle n_F\rangle^2}. \tag{52}$$

As can be seen in Fig. 21, where the correlation strength b at $\sqrt{s} = 200$, 546, and 900 GeV is plotted as a function of the gap size $\Delta\eta$, LIPJET reproduces the variation of b with $\Delta\eta$ and with the energy.

F. Two-particle correlations in the azimuthal angle

It was proposed by Wang [51], to study the role of minijets in high energy hadronic interactions via the normalized two-particle correlation in the azimuthal angle ϕ:

$$C(\phi_1,\phi_2) = \frac{\rho(\phi_1,\phi_2)}{\rho(\phi_1)\rho(\phi_2)} - 1, \tag{53}$$

where $\rho(\phi)$ is the single- and $\rho(\phi_1,\phi_2)$ the two-particle density in ϕ. It was argued in Ref. [51] that calculating $C(\phi_1,\phi_2)$ for samples of particles with $p_\perp \geq p_\perp^{\rm cut}$, the influence of the underlying "soft" interaction on this correlation can be reduced. The higher the $p_\perp^{\rm cut}$, the more the correlation should look like the profile of high $p_\perp$ jets. In Fig. 22, $C(0,\Delta\phi)$ calculated by LIPJET for $p_\perp^{\rm cut} = 0$, 0.5,

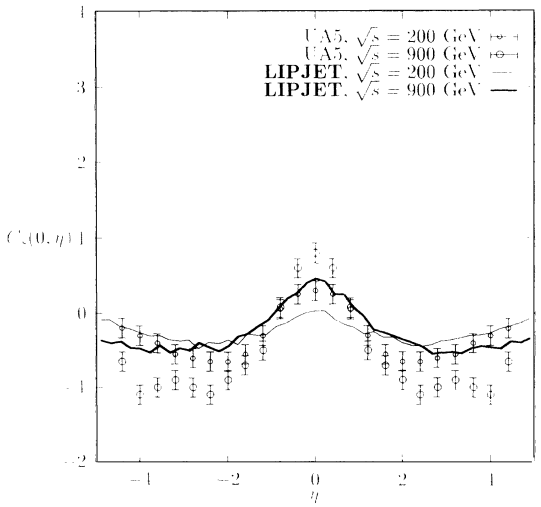

FIG. 20. The two-particle "short range" correlation function $C_s(0,\eta)$ at $\sqrt{s} = 200$ and 900 GeV. The lines correspond to the LIPJET calculation, the points to the UA5 data [50].

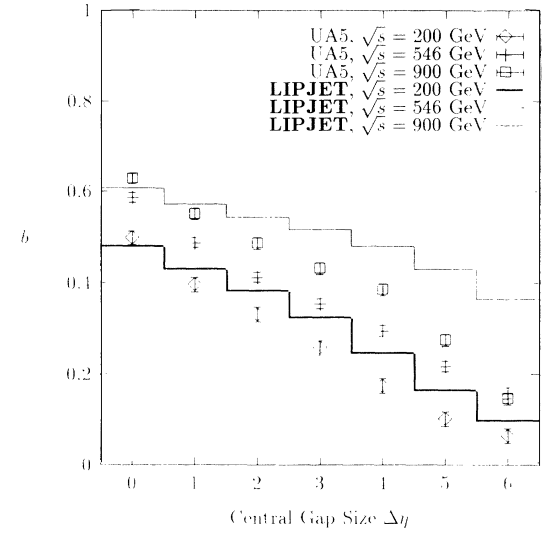

FIG. 21. The strength of the forward-backward correlation at $\sqrt{s} = 200$, 546, and 900 GeV as a function of the central gap size $\Delta\eta$. The lines represent the results from our model, the points are from Ref. [50].

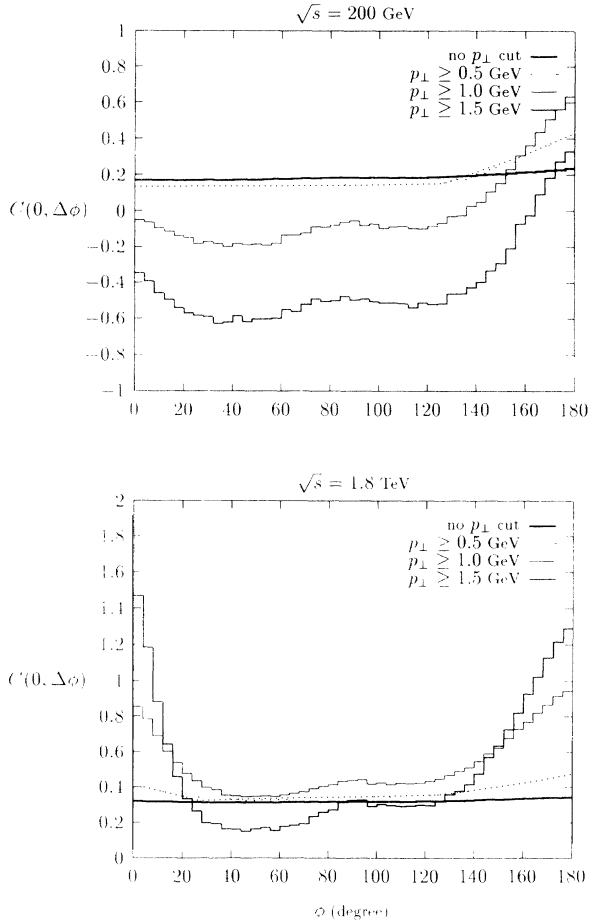

FIG. 22. The two-particle correlation in the azimuthal angle $C(0,\Delta\phi)$ calculated for different values of the $p_\perp^{\rm cut}$ in the whole rapidity range.

1.0, and 1.5 GeV in the whole rapidity range is shown for $\sqrt{s}$ =200 and 1800 GeV. We find a qualitative agreement with the results of Ref. [51]. Unlike high $p_\perp$ back-to-back jets which are both kinematically bound to the central rapidity region, in my model minijets can be easily produced with a large rapidity gap between them. Therefore if we calculate the two-particle correlation in a limited rapidity window, the minijet contribution to $C(0, \Delta\phi = \pi)$ (from events, where a pair of minijets is produced) will mostly drop out, but the contribution to $C(0, \Delta\phi = 0)$ still remains. Shown in Fig. 23 is $C(0, \Delta\phi)$ calculated in $|\eta| \leq 1$. As expected, the correlation at $\Delta\phi = \pi$ is reduced as compared to Fig. 22.

So far my results are in qualitative agreement with the calculations with the model HIJING [51]. However, in HIJING the multigluon intermediate state of the reaction is obtained through multiple $2 \to 2$ parton scattering. Therefore, every parton pair is moving back-to-back. This implies a stronger correlation at $\Delta\phi = \pi$ as in my model, where the multigluon intermediate state is obtained from the equation of the PP and a considerable fraction of the cut Pomerons has more then two s-channel gluons. Let me clarify this feature in a simple toy model where particle production proceeds only via independent $2 \to 2$ parton scatterings and the hadrons from a parton are perfectly bundled in the parton direction. If we now assume that the hadron multiplicity distribution from a jet pair has a Poisson form (as, for example, done in Ref. [52]) with an average multiplicity $\bar{n}_{\text{jet}}$, we get an average contribution to the two-particle distribution $\rho(0, \pi)$ equal to $\bar{n}^2_{\text{jet}}/4$ and an average contribution to $\rho(0, 0)$ equal to $\bar{n}^2_{\text{jet}}/4 - \bar{n}_{\text{jet}}/2$. With this, it is clear that in the considered toy model the two-particle correlation for $\Delta\phi = \pi$ will be ever stronger as for $\Delta\phi = 0$. Indeed, in reality the particles from a minijet are smeared over some ϕ region. Furthermore, in HIJING initial and final state radiation is included. Therefore, in [51] it was found that

$$\Delta C(\pi) = C(0, \Delta\phi = 0) - C(0, \Delta\phi = \pi) \tag{54}$$

approaches zero at energies above the Tevatron. In Fig. 24(a) $\Delta C(\pi)$ as calculated by LIPJET is plotted as a function of $\sqrt{s}$. It can be seen that in my model $\Delta C(\pi)$ grows continuously with the energy and does not show saturation up to SSC energy for $p_\perp^{\text{cut}} \geq 1$ GeV. Moreover, for $p_\perp = 1.5$ GeV $\Delta C(\pi)$ is greater than zero already at $\sqrt{s} \approx 1$ TeV. The difference between my model and the results presented in [51] is even more comprehensive if we consider

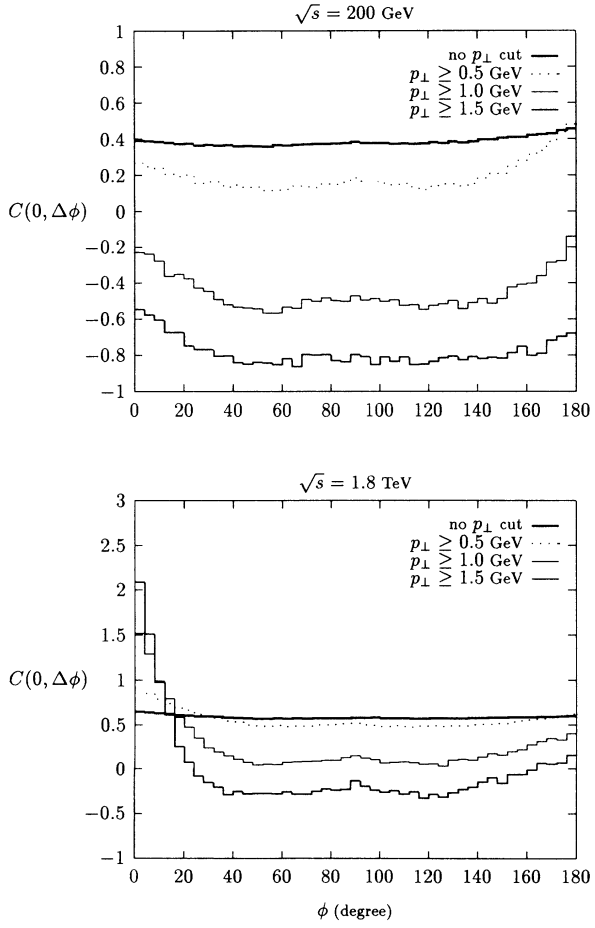

FIG. 23. The same as in Fig. 22 but calculated in $|\eta| \leq 1$.

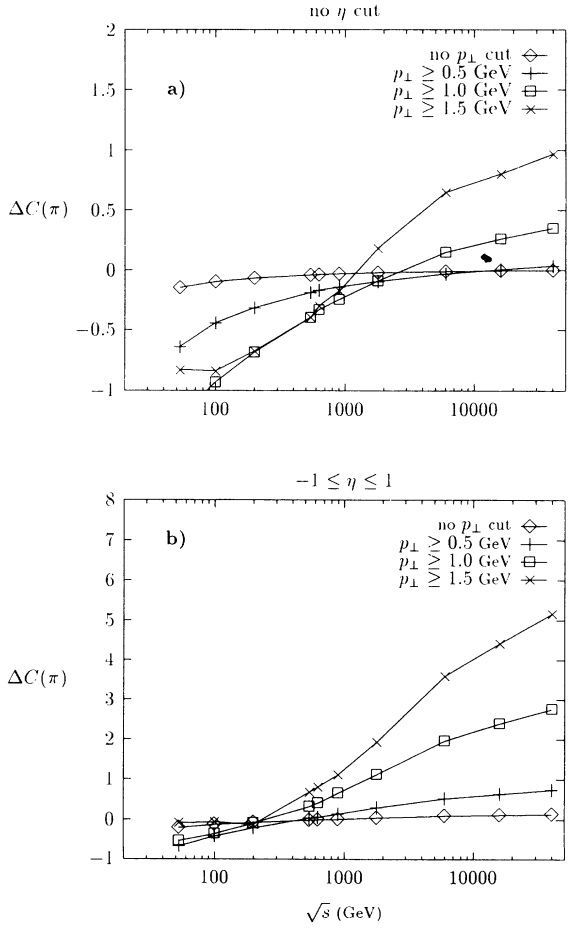

FIG. 24. The difference between the two-particle correlation $C(0, \Delta\phi)$ at $\Delta\phi = 0$ and $\Delta\phi = \pi$ as a function of the c.m.s. energy. (a) Calculation with no η cut, (b) calculation for $|\eta| \leq 1$.

$$\Delta C(\pi/3) = C(0, \Delta\phi = 0) - C(0, \Delta\phi = \pi/3). \quad (55)$$

$\Delta C(\pi/3)$ measures the contribution to the two-particle correlation of the minijets as compared to the background. Contrary to what was found in Ref. [51], in my model $\Delta C(\pi/3)$ increases with energy up to $\sqrt{s} = 40$ TeV independent of the $p_\perp^{\rm cut}$ applied as can be seen in Fig. 25(a). For completeness, $\Delta C(\pi)$ and $\Delta C(\pi/3)$ calculated in a limited rapidity range $|\eta| \leq 1$ are shown in Figs. 24(b) and 25(b).

In this subsection, the difference between my model and a model where the multiparton intermediate state of high energy hadronic interactions is described in the form of multiple independent $2 \to 2$ scatterings is clearly demonstrated. It can be concluded that the systematic experimental study of the two-particle correlation in the azimuthal angle ϕ may provide a powerful tool to reveal the properties of the underlying dynamics.

VI. SUMMARY AND OUTLOOK

In the present paper it was shown that the equation of the PP resulting from the summation of all orders of PQCD in the LLA can be used to construct a simulation procedure for the multigluon intermediate state of high energy hadronic interactions. With a simple and rather general ansatz for the coupling of the PP on the hadrons, the intercept of the Pomeron containing both "soft" and perturbative contributions was expressed in terms of the trajectory of the Reggeized gluon calculated with a given regularization cutoff μ. In this manner, no additional assumptions are necessary to obtain the relative weights of the "soft" and the perturbative part of the interaction. Moreover, in the presented model the intermediate gluon state in the case of a "pure" soft situation differs from the driving term of the perturbative expansion only by the transverse momentum exchange by the t-channel Reggeized gluon, being $< \mu$ in the first case and $\geq \mu$ in the second.

Unitarity corrections to the single Pomeron amplitude and the exclusive multi-Pomeron cross sections necessary to describe particle production are calculated in the framework of perturbative Reggeon calculus in the presented model. An excellent description of the total and elastic cross sections and the ratio of the real to the imaginary part of the elastic scattering amplitude is obtained.

Implementing the model in the form of a Monte Carlo event generator, particle production in $p\bar{p}$ collisions was studied in the energy range from $\sqrt{s} = 50$ GeV up to the energy of the SSC. A reasonable agreement with a wealth of experimental data was found. Let me mention the increase of the average charged multiplicity, the multiplicity distributions and the violation of the KNO scaling, the rise of the pseudorapidity density at $\eta = 0$ with the energy, the pseudorapidity and transverse momentum distributions, and the increase of the correlations among the final state particles. The detailed study of intermittency within the model will be presented in a separate paper.

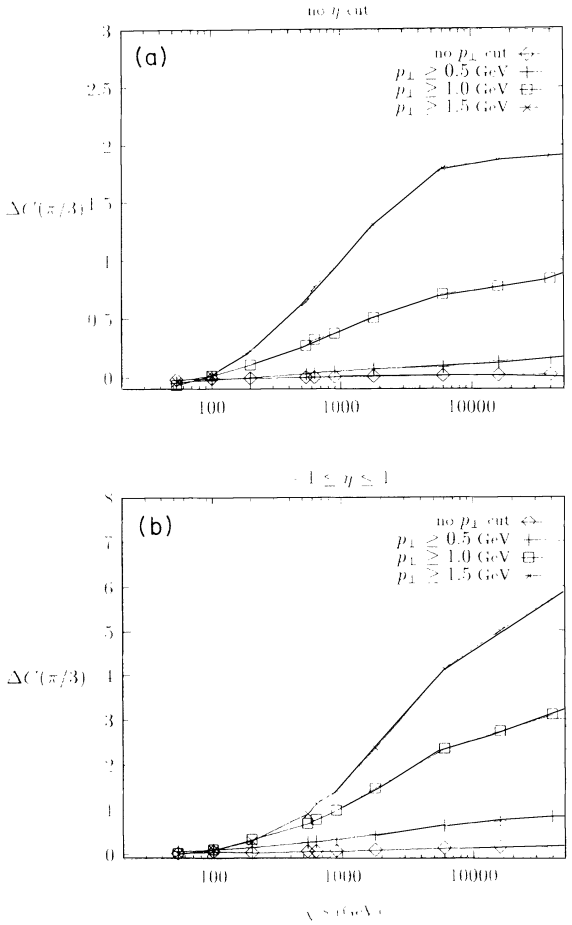

FIG. 25. The difference between the two-particle correlation $C(0, \Delta\phi)$ at $\Delta\phi = 0$ and $\Delta\phi = \pi/3$ as a function of the c.m.s. energy. (a) Calculation with no η cut, (b) calculation for $|\eta| \leq 1$.

It has been shown that the differences of the presented model, where all orders of PQCD in the LLA are simultaneously taken into account to a model, where the multigluon intermediate state of the collision results from multiple independent $2 \to 2$ scatterings with associated initial and final state radiation can be studied via the two-particle correlation in the azimuthal angle.

Finally, I want to note that in the framework of a vector dominance model (VDM), the model can be applied to study particle production in γp collisions without any additional assumptions. A forthcoming paper [53] on this is planned.

ACKNOWLEDGMENTS

I acknowledge useful discussions with R. Kirschner, M. Fippel, J. Ranft, and R. Engel. I am grateful to R. Engel, H. J. Möhring and J. Ranft for many helpful remarks on this manuscript.

[1] A. Capella and J. Tran Thanh Van, Z. Phys. C **23**, 165 (1984).
[2] A . Capella, J. Tran Thanh Van, and J. Kwiecinski, Phys. Rev. Lett. **58**, 2015 (1987).
[3] T. K. Gaisser and F. Halzen, Phys. Rev. Lett. **54**, 1754 (1985).
[4] J. Durand and H. Pi, Phys. Rev. Lett. **58**, 2015 (1987).
[5] G. Pancheri and Y. N. Srivastava, Phys. Lett. B **182**, 199 (1986).
[6] F. W. Bopp, A. Capella, J. Ranft, and J. Tran Thanh Van, Z. Phys. C **51**, 99 (1991).
[7] P. Aurenche, F. W. Bopp, A. Capella, J. Kwiecinski, M. Maire, J. Ranft, and J. Tran Thanh Van, Phys. Rev. D **45**, 92 (1992).
[8] X.-N. Wang and M. Gyulassy, Phys. Rev. D **45**, 844 (1992).
[9] R. Engel, F. W. Bopp, D. Pertermann, and J. Ranft, Phys. Rev. D **46**, 5192 (1992).
[10] X. N. Wang and M. Gyulassy, Phys. Rev. D **44**, 3501 (1991).
[11] T. Söstrand and M. van Zijl, Phys. Rev. D **36**, 2019 (1987).
[12] B. Andersson, G. Gustafson, and B. Nilsson-Almqvist, Nucl. Phys. **B281**, 289 (1987).
[13] E. A. Kuraev, L. N. Lipatov, and V. S. Fadin, Phys. Lett. **60B**, 50 (1975).
[14] E. A. Kuraev, L. N. Lipatov, and V. S. Fadin, Zh. Eksp. Teor. Fiz. **71**, 81 (1976).
[15] E. A. Kuraev, L. N. Lipatov, and V. S. Fadin, Zh. Eksp. Teor. Fiz. **72**, 577 (1977).
[16] V. N. Gribov, Zh. Eksp. Teor. Fiz. **53**, 654 (1967) [Sov. Phys. JETP **26**, 414 (1968)].
[17] A. Capella, U. Sukhatme, and J. Tran Thanh Van, Phys. Lett. **81B**, 68 (1979).
[18] A. Capella, U. Sukhatme, and J. Tran Thanh Van, Z. Phys. C **3**, 329 (1980).
[19] A. Capella, U. Sukhatme, C. I. Tan, and J. Tran Thanh Van, Z. Phys. C **10**, 249 (1981).
[20] A. Capella, U. Sukhatme, C. I. Tan, and J. Tran Thanh Van, Phys. Lett. **114B**, 450 (1982).
[21] A. Capella, U. Sukhatme, C. I. Tan, and J. Tran Thanh Van, Orsay Report No. LPTHE 92–38, 1992 (unpublished).
[22] M. Fippel and R. Kirschner, Phys. Rev. D **48**, 2035 (1993).
[23] I. Kawrakow, Ph.D. thesis, University of Leipzig.
[24] L. N. Lipatov, Zh. Eksp. Teor. Fiz. **90**, 1536 (1986) [Sov. Phys. JETP **63**, 904 (1986)].
[25] R. Kirschner and L. N. Lipatov, Z. Phys. C **45**, 477 (1990).
[26] R. Kirschner (private communication).
[27] A. Donnachie and P. V. Landshoff, Nucl. Phys. **B231**, 189 (1983).
[28] A. Donnachie and P. V. Landshoff, Phys. Lett. B **296**, 227 (1993).
[29] P. D. B. Collins and F. D. Gault, Phys. Lett. B **188**, 143 (1978).
[30] P. D. B. Collins, *An Introduction to Regge Theorie & High Energy Physics* (Cambridge University Press, Cambridge, England, 1977).
[31] See references in M. M. Block, F. Halzen, and B. Margolis, Phys. Lett. B **252**, 481 (1990); M. M. Block and A. R. White, *ibid.* **273**, 145 (1991).
[32] V. A. Abramovski, V. N. Gribov, and O. V. Kancheli, Yad. Fiz. **18**, 595 (1973) [Sov. J. Nucl. Phys. **18**, 308 (1973)].
[33] UA1 Collaboration, C. Albajar *et al.*, Nucl. Phys. **B309**, 405 (1988).
[34] J. Ranft and S. Ritter, Acta Phys. Pol. B **11**, 259 (1980).
[35] S. Ritter, Comput. Phys. Commun. **31**, 393 (1984).
[36] B. Andersson, G. Gustafson, G. Ingelman, and T. Söstrand, Phys. Rep. **97**, 31 (1983).
[37] T. Söstrand, Comput. Phys. Commun. **27**, 243 (1982).
[38] ABCDHW Collaboration, A. Breakstone *et al.*, Phys. Rev. D **30**, 528 (1984).
[39] UA5 Collaboration, R. E. Ansorge *et al.*, Z. Phys. C **43**, 357 (1989).
[40] UA5 Collaboration, G. J. Alner *et al.*, Phys. Lett. **160B**, 193 (1985); **160B**, 199 (1985).
[41] E735 Collaboration, C. S. Lindsey *et al.* in *Quark Matter '91*, Proceedings of the Ninth International Conference on Ultrarelativistic Nucleus-Nucleus Collisions, Gatlinburg, Tennessee, edited by T. C. Awes *et al.* [Nucl. Phys. A **544**, 343 (1992)].
[42] UA5 Collaboration, G. J. Alner *et al.*, Z. Phys. C **33**, 1 (1986).
[43] CDF Collaboration, F. Abe *et al.*, Phys. Rev. D **41**, 2330 (1990).
[44] UA1 Collaboration, C. Albajar *et al.*, Nucl. Phys. **335**, 261 (1990).
[45] UA7 Collaboration, E. Pare *et al.*, Phys. Lett. B **242**, 531 (1990).
[46] UA5 Collaboration, R. E. Ansorge *et al.*, Z. Phys. C **41**, 179 (1988).
[47] UA5 Collaboration, G. J. Alner *et al.*, Nucl. Phys. **B258**, 505 (1985).
[48] E. Berger, Nucl. Phys. **B85**, 61 (1975).
[49] J. Ranft, Fortschr. Phys. **23**, 467 (1975).
[50] UA5 Collaboration, R. E. Ansorge *et al.*, Z. Phys. C **37**, 191 (1988).
[51] X. N. Wang, Phys. Rev. D **47**, 2754 (1993).
[52] X. N. Wang, Phys. Rev. D **43**, 104 (1991).
[53] R. Engel and I. Kawrakow (unpublished).